PNAS
www.pnas.org

Supplementary Information for

Responsive manipulation of neural circuit pathology by fully implantable, front-end multiplexed embedded neuroelectronics

Zifang Zhao, Claudia Cea, Jennifer N. Gelinas*, Dion Khodagholy*

*Jennifer Gelinas
Email: jng2146@cumc.columbia.edu
*Dion Khodagholy
Email: dk2955@columbia.edu

This PDF file includes:

Figures S1 to S13

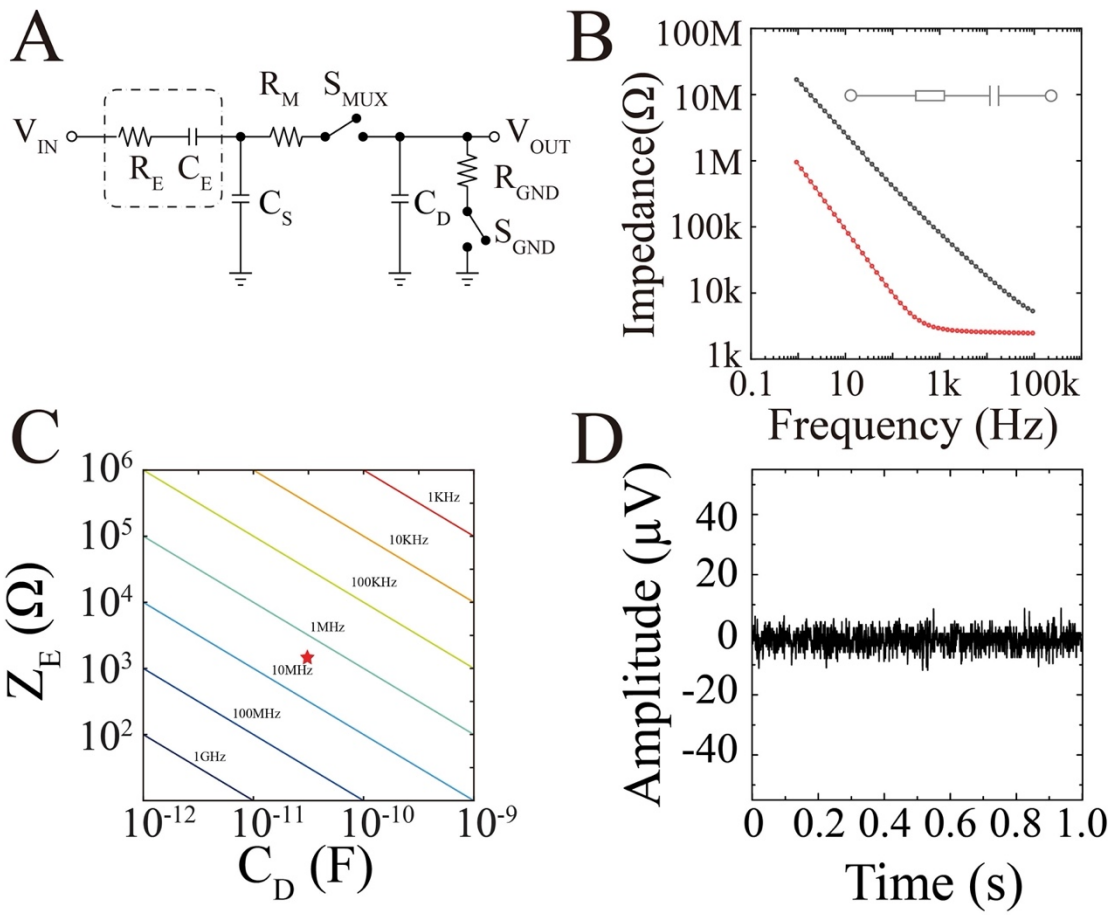

Supplementary Figure 1: High charge capacity of multi-electrodes and low drain capacitance switching enable multiplexing prior to amplification.

A. Detailed circuit diagram of MTA device consisting of an RC (R_E and C_E) model representing an electrode (Z_E, dashed box), and a switch (S_{MUX}) with the line resistance (R_M), drain (C_D) and source (C_S) parasitic capacitances forming a multiplexer. R_{GND} and S_{GND} represent the charge drainage pathway.
B. Electrochemical impedance spectroscopy for a 50 μm diameter tungsten wire (black) and a PEDOT:PSS coated electrode (red). Schematic of the simplified RC circuit of the electrodes (inset; C_W = 280 pF, $C_{PEDOT:PSS}$ = 70 nF).
C. The cut-off frequency (colored diagonal lines) of the system defined by Z_E and C_D. Red star indicates the experimental values in this work.
D. Sample raw trace of an MTA-based recording using a 50 μm tungsten wire inside a grounded (Ag/AgCl) PBS bath (RMS = 7.27 μV).

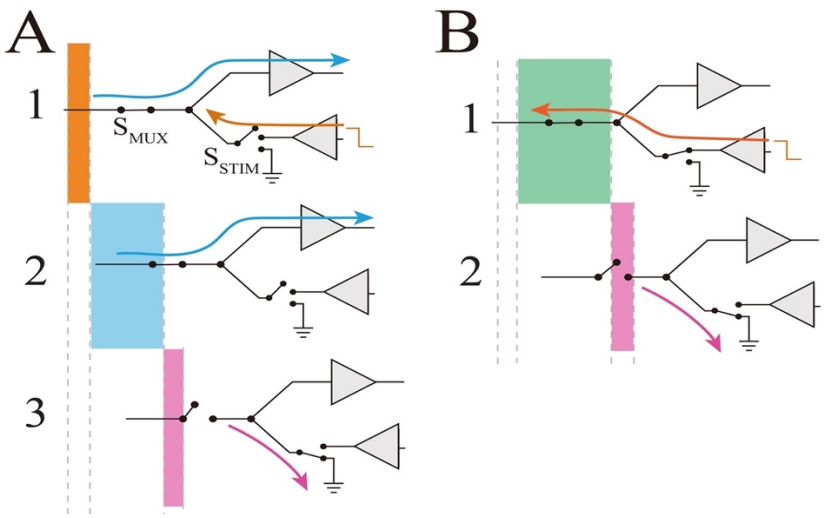

Supplementary Figure 2: Schematic of recording and stimulation sequences.

A. For acquisition:
   1. S_{MUX} is closed, S_{STIM} is open and the stimulating amplifier compensates the charge injection of S_{STIM} closure through S_{STIM} off-capacitance.
   2. S_{MUX} is closed, S_{STIM} is open, and the acquisition path directs the electrode voltage to the amplifier.
   3. S_{MUX} is open, S_{STIM} is closed to the ground for a short period of time to drain the residual charge in the S_{MUX}.

B. For stimulation:
   1. S_{MUX} is closed, S_{STIM} is closed to the stimulation amplifier allowing the stimulation path to direct the stimulation voltage to the electrode.
   2. S_{MUX} is open, S_{STIM} is closed to the ground for a short period of time to drain the residual charge in the S_{MUX}.

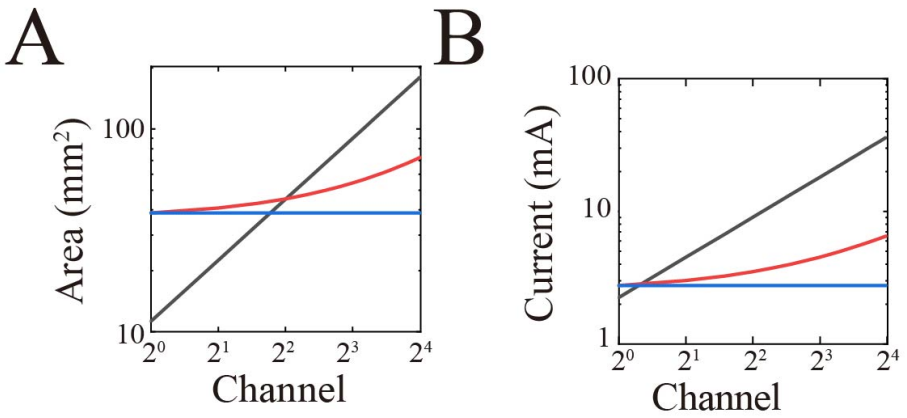

Supplementary Figure 3: MTA decreases physical form factor and lowers power consumption compared to conventional designs.

A. Comparison of circuit form factor required for un-multiplexed (black), conventional multiplexed circuit (red) and MTA-based circuit (blue) as a function of number of channels. The un-multiplexed circuit has small area at very low channel counts due to absence of any multiplexing block. As number of channels increases, the conventional multiplexed circuit has stable area until the number of channels per individual multiplexer is exceeded, after which it increases non-linearly. The MTA design provides most efficient area usage as channel number increases. Note: amplifier and multiplexing component characteristics represented in this figure are derived from components used in the MTA and shown the device schematic (**Supplementary Figure 4**).

B. Comparison of current consumption of the un-multiplexed (black), conventional multiplexed circuit (red) and MTA-based circuit (blue) as a function of number of channels. For single channel acquisition, the un-multiplexed circuit has slightly lower power consumption as no multiplexer is needed. However, as number of channels increases, power consumption for this circuit increases dramatically relative to the multiplexed systems. Importantly, the MTA-based circuit maintains a very similar power consumption that is independent of channel count and significantly lower than that of conventional multiplexed circuits.

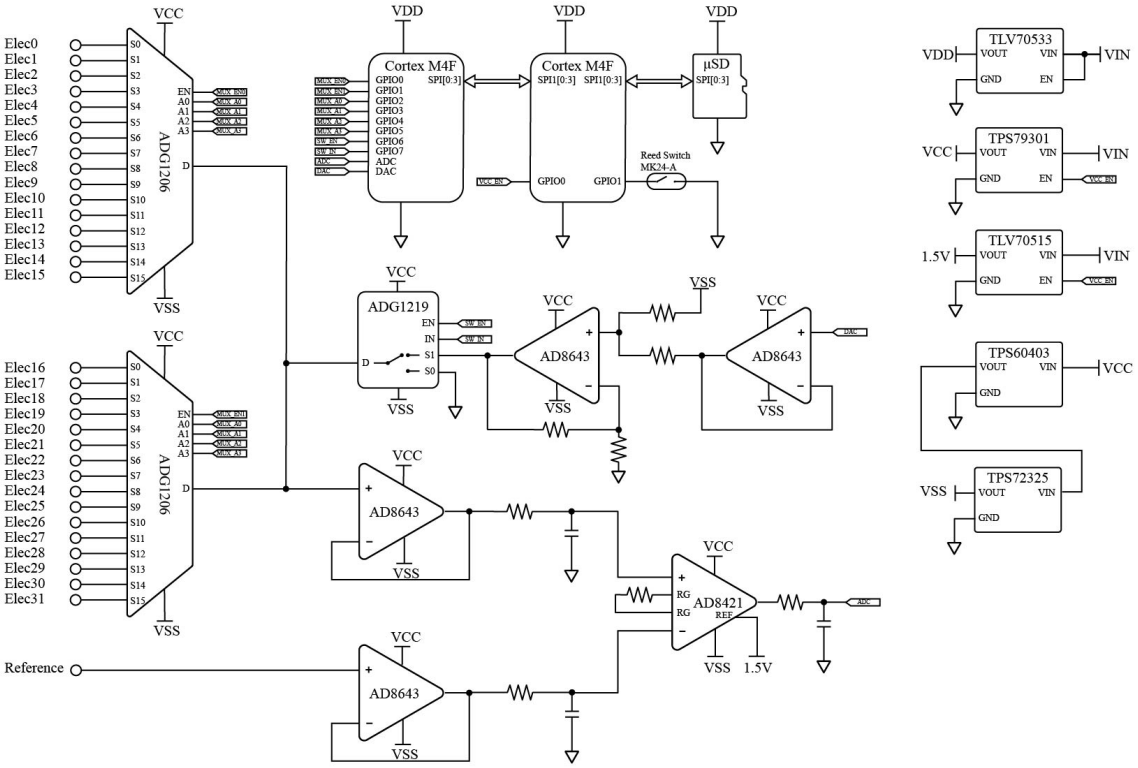

Supplementary Figure 4: Full schematic of MTA-based neural embedded neuroelectronics.

Complete schematic including the individual component part numbers and their logical connections. The circuits on the right side of the schematic perform power conversion and management using low-drop regulators and charge pumps for establishing negative voltage rail.

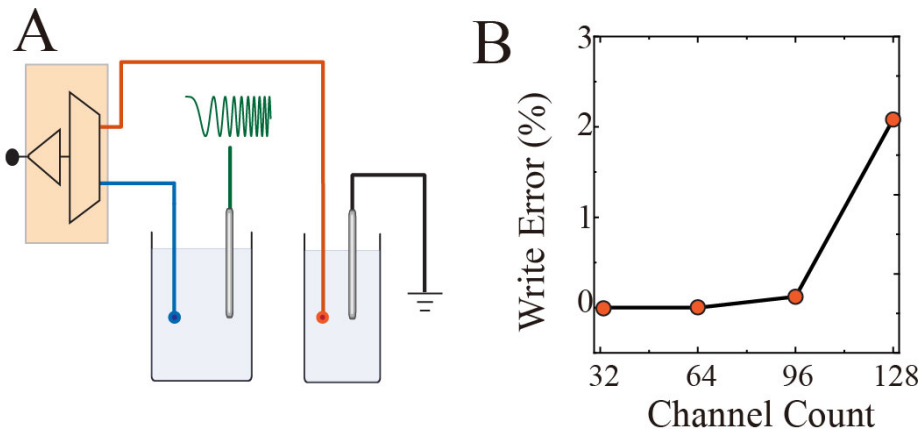

Supplementary Figure 5: Stable *in vitro* data acquisition and transmission using MTA.

A. Schematic of experimental setup for evaluating the stability of MTA-based circuits (**Figure 2c**). The recording electrode (blue) placed in the same chamber as the stimulating electrode (orange) captured the sweep signal (green trace; 500 µV, 1-500 Hz, 120 s) while the recording electrode associated with the adjacent MTA channel (orange) placed in the second chamber did not.

B. Error rate defined by percentage of missing or incorrect bits per package over the course of 1 h of MTA recording. The received data was validated against a known sequence of data (ideal ramp increments from 0 to 2^{12}).

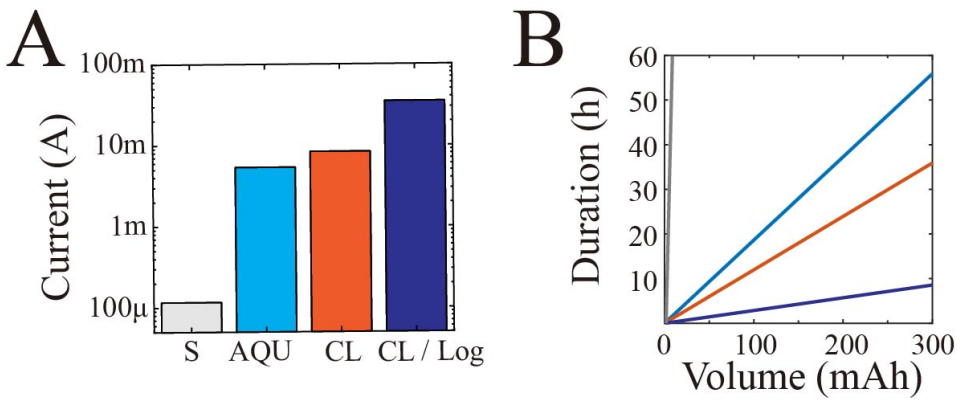

Supplementary Figure 6: Power consumption characteristics of MTA device during various modes of operation.

A. Comparison of current consumption during various modes of MTA-based embedded system operation. S stands for standby; AQU for acquisition; CL for closed-loop; CL/Log for closed loop while writing data into the internal memory.
B. Comparisons of duration of device operation during various modes as a function of battery capacity. Standby (gray), acquisition (light blue), closed-loop (orange), closed-loop while writing data into the internal memory (dark blue). The current system with 80 mAh and 135 mAh batteries was able to perform closed-loop recording, stimulation, and data logging for 2.2 and 4.7 hours, respectively. We estimate continuous responsive neurostimulation could be performed for 9.4 h and 15.5 h, respectively.

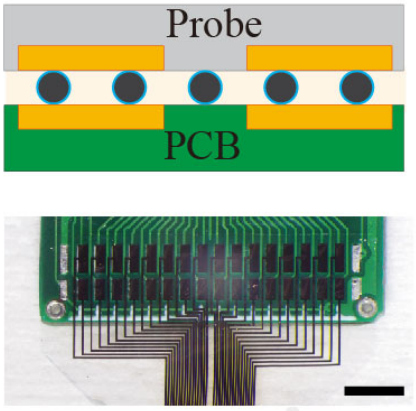

Supplementary Figure 7: MCP-based bonding of conformable array to printed circuit board.

Cross-sectional schematic of the MCP (black circles) acting as an anisotropic conductive film between the probe and a PCB (top). Micrograph of the back-end of a conformable implantable probe directly bonded using MCP onto a 250 µm thick PCB prior to encapsulation (Scale bar, 5 mm).

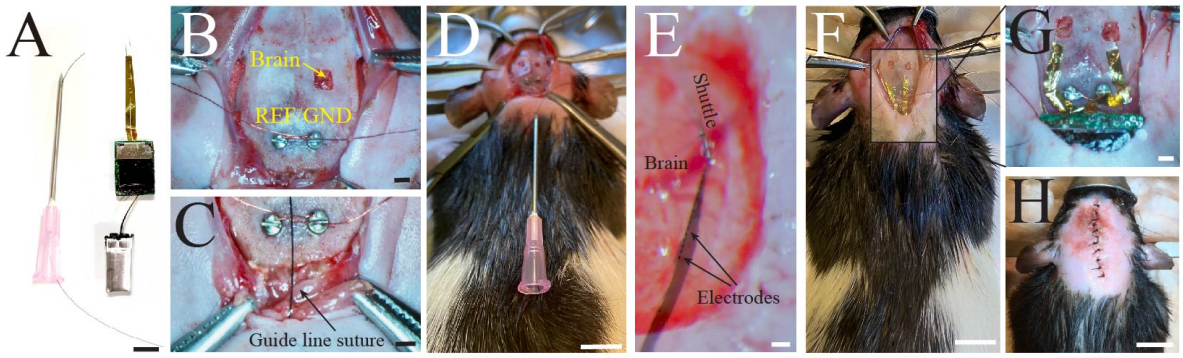

Supplementary Figure 8: Procedure for implantation of conformable arrays into the rat brain for subsequent chronic neurophysiologic recording.

A. Photograph of embedded device prepared for implantation with trocar. Scale bar, 10 mm.
B. Photograph of skull with reference/ground screws implanted over cerebellum and craniotomy drilled in preparation for array implantation. Scale bar, 1 mm.
C. Photograph showing guide line suture that will be used to pull MTA device into position in the subcutaneous space. Scale bar, 1 mm.
D. Photograph showing needle used as trocar to tunnel MTA device into implantation position. Scale bar, 10 mm.
E. Photograph of conformable implantable probe being penetrated into brain using a shuttle. Individual electrodes are visible; scale bar, 50 µm.
F. Photograph of MTA device and conformable probes in implanted position. Scale bar, 10 mm.
G. Micrograph of implanted MTA device from Figure 3A. Scale bar, 1 mm.
H. Photograph showing post-operative appearance of MTA implantation. Scale bar, 10 mm.

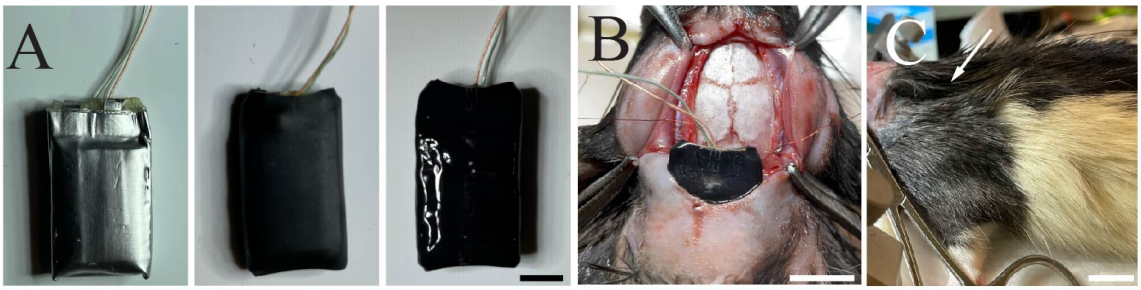

Supplementary Figure 9: Procedure for encapsulation and implantation of 135 mAh battery.

A. Bare off-the-shelf battery (left); encapsulated battery using thermoplastic to eliminate sharp edges and provide further mechanical support (middle); fully encapsulated battery using implantable grade silicone adhesive (Nusil MED-1137; right); scale bar 2 mm.
B. Optical micrograph of the battery during implantation in the subcutaneous space using the trocar approach demonstrated in **Supplementary Figure 8.** Scale bar 5 mm.
C. Fully implanted battery secured in the subcutaneous space. White arrow indicates the location of the battery. Scale bar 10 mm.

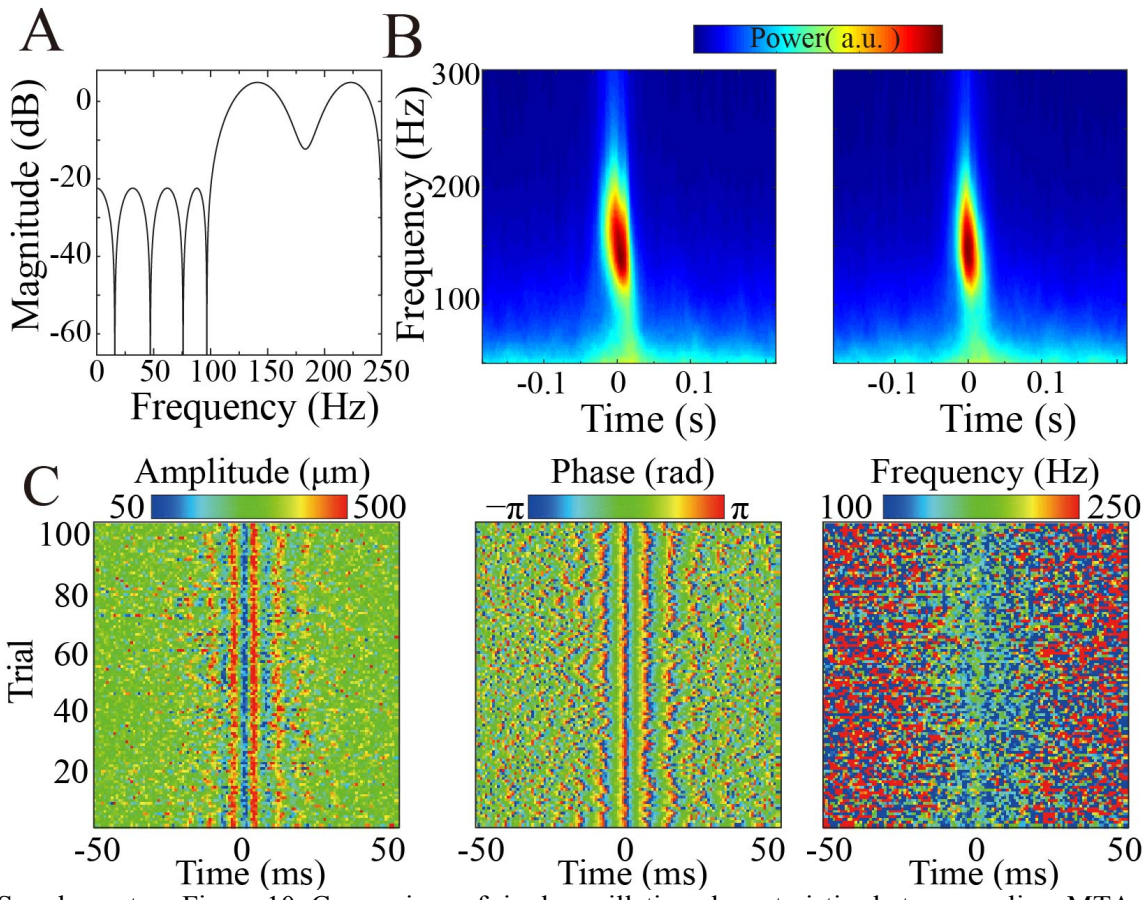

Supplementary Figure 10: Comparison of ripple oscillation characteristics between online, MTA-based detection and off-line detection.

A. Bode plot of a bandpass filter employed in closed-loop ripple detection.
B. Normalized spectrograms of ripples detected using online MTA-based and offline detections during one recording session (n = 200 ripples).
C. Stacked 100 successive trials of online-detected ripples visualized in terms of amplitude, phase, and frequency, highlighting the consistent waveform characteristics and detected onset time.

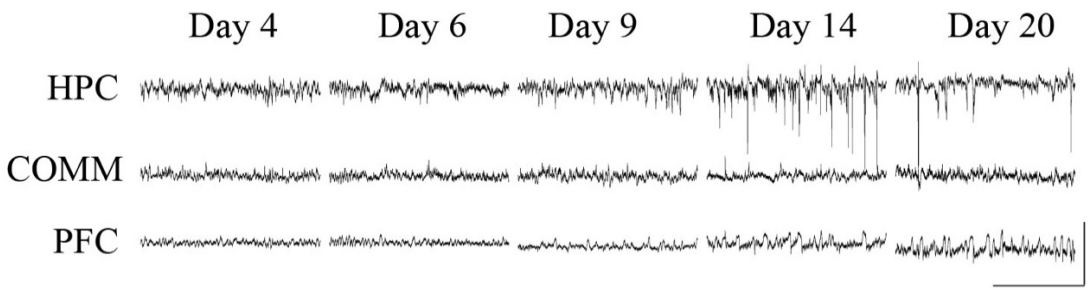

Supplementary Figure 11: MTA-based device enables stable *in vivo* data acquisition and logging.

Sample raw LFP traces for the same animal over the course of kindling. Note the emergence of large amplitude negative discharges in later days (day 14, 20) that are characteristic of IEDs. Scale bar 5 s, 1 mV.

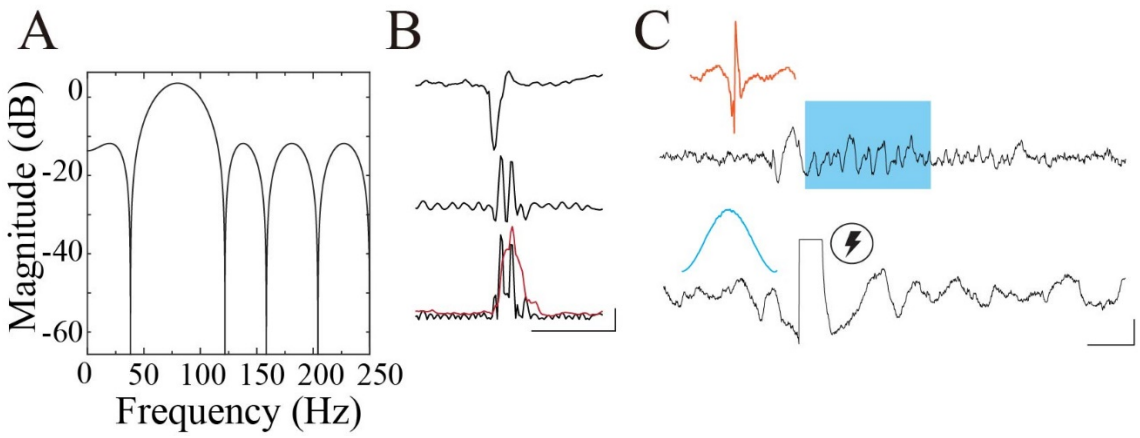

Supplementary Figure 12: MTA enables controllable filter properties for real-time online detection filters.

A. Bode plot of a bandpass filter employed in IED closed-loop detection.
B. Main signal processing steps involved during IED detection. From top to bottom: wideband LFP, bandpass-filtered LFP, rectified filtered LFP (black), smoothed envelope (red). Scale bar: 100 ms, 100 μV.
C. Representative IED-triggered LFP in mPFC without (top; blue box = IED-induced spindle) and with effective spindle suppression protocol (bottom). Scale bar, 500 ms, 100 μV. Note: the ADC clipping circuit is activated during gaussian stimulation and no recording is performed during the stimulation time.

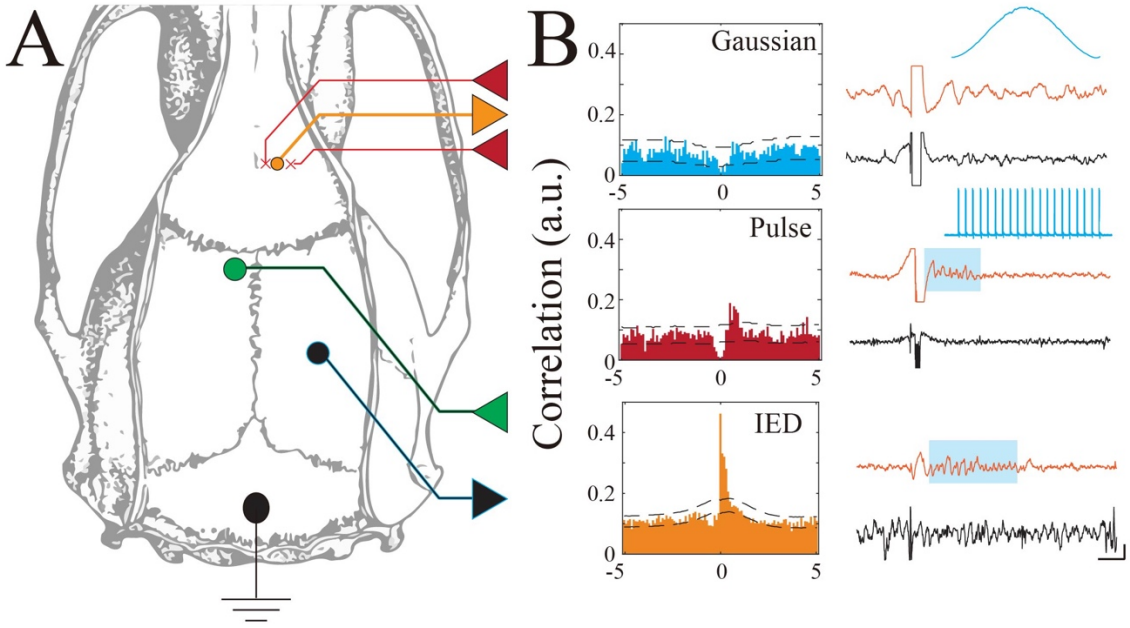

Supplementary Figure 13: Comparison of various real-time, closed-loop stimulation protocols on pathological hippocampal-cortical coupling.

A. Experimental setup illustrating the placement of recording and stimulating electrodes. Recording arrays are placed in each of the hippocampus (blue) and mPFC (orange). Two of the recording electrodes implanted in mPFC are used as a bipolar stimulation electrode pair (red). Stimulation of hippocampal commissure (green) kindles the rat, leading to spontaneous hippocampal IEDs.

B. Cross-correlograms of hippocampal IEDs and mPFC spindles with and without closed-loop stimulation (blue = gaussian stimulation, n = 1492 from 4 animals; red = pulse stimulation, n = 2897 from 4 animals; orange = unmodified IED, n = 6342 from 4 kindled animals). Dashed lines correspond to 95% confidence intervals. Right column shows corresponding LFP traces in mPFC (orange) and hippocampus (black) with blue traces showing applied stimulation waveform. Blue boxes show detected spindles. Scale bar 200 ms, 100 µV.